IL NUOVO CIMENTO Vol. 36 C, N. 4 Luglio-Agosto 2013
DOI 10.1393/ncc/i2013-11536-0

Communications: SIF Congress 2012

Access to particle-particle emitting sources at intermediate energies

E. V. Pagano

Dipartimento di Fisica e Astronomia, Università di Catania - Catania, Italy and INFN-Laboratori Nazionali del Sud - Via S. Sofia, Catania, Italy

ricevuto il 10 Gennaio 2013

Summary. — The study of nuclear matter under extreme conditions is a very active area in nuclear physics. This study may improve our understanding of the equation of states and liquid-gas phase transitions in nuclear matter as well as the spectroscopic and dynamic characterization of exotic nuclear systems and reactions. A clear characterization of nuclear interacting systems requires probing the space-time properties of various particle-emitting sources and the knowledge of the reaction mechanism. Particle-particle correlations represent a very powerful technique to study emitting sources produced during a reaction. In this work two-proton correlation functions measured in Xe+Au at $E = 50\,\mathrm{MeV/nucleon}$ have been studied. By using angle-averaged two-proton correlation functions and imaging techniques we have estimated some of the basic proprieties, such as the size and the relative contributions provided by two-particle–emitting sources produced in semi-central collisions and characterized by different emission time-scales.

PACS 25.70.-z – Low and intermediate energy heavy-ion reactions.
PACS 25.70.Pq – Multifragment emission and correlations.

1. – Introduction

The study of the dynamics of nuclear reactions in heavy-ion collisions is a very active area in nuclear physics. In fact, depending on the beam energy, one is faced with different time-scales of the response of the nucleus to the excitation of the relevant (energy dependent) degrees of freedom. This opens the possibility to explore systems with densities lower or larger than the one of nuclear matter at saturation ($\rho_0 = 0.17\,\mathrm{nucleon/fm^3}$).

At Fermi energies, between $20\,\mathrm{MeV}/u$ and $200\,\mathrm{MeV}/u$, within time-scales of the order of $100\,\mathrm{fm}/c$, the dynamical phase of a violent head-on collision experiences a collective compression where the overlapping nuclear density is predicted [1, 2] to achieve values above the value of the saturation density. Then, the evolution is predicted to undergo an expansion phase where the density goes down to significant lower values (of the order of 0.3 ρ_0, freeze-out phase) and a rapid multi-fragmentation of the system in many

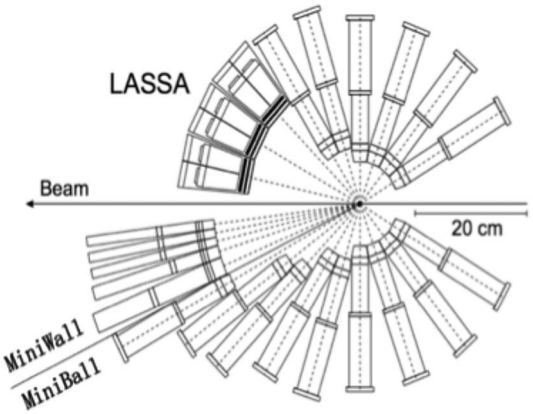

Fig. 1. – The Experimental setup, LASSA + Miniball/Miniwall.

excited clusters and light particles takes place. It is still a fundamental open question if at freeze-out the system achieves full equilibrium or not. However, clear evidence of secondary decays coming from excited fragments has been established [3-5]. It is within this very complex scenario that experimental methods and techniques for probing space-time property of the different emitting sources have been developed. Among the various techniques introduced in nuclear science in order to probe both the dynamics and the equilibrium phase of the reactions, correlation functions and intensity interferometry play a key role [6]. In the following sections, basic properties of the particle-particle correlation techniques will be briefly discussed and applied to the study of a specific reaction system.

2. – Experimental method

Early in nuclear reaction studies, scientists were faced with the crucial problem to disentangle among different time-scales of the reaction that are involved in the same collision process [7]. Indeed, in order to well understand nuclear interactions one has to take into account both the emitting sources that are created during the collision dynamics and the ones that are sequentially emitted over time-scales orders of magnitude longer than the prompt ones involved in the collision process. This problem is very complex because the dynamics of the reaction depends on different parameters. For example the incident energy of the beam, the centrality of the collision (impact parameter), the mass of the system, etc., are crucial parameters. In this work special attention is paid to Fermi Energy domain of the collision scenario. In particular, the study is devoted to select quasi-central collisions in the reaction $^{129}\mathrm{Xe} + {}^{197}\mathrm{Au}$ at $E/A = 50\,\mathrm{MeV/nucleon}$. The experimental interferometry analysis concerns with data collected in an experiment that was performed at Michigan State University (MSU) and the experimental setup was composed of LASSA coupled to the Miniball/Miniwall array sketched on fig. 1. LASSA is a particle-particle correlator made by three stages of detection. The first stage is a silicon strip detector with 16 vertical strips in the front side with a $65\,\mu$m thickness; the second one is a DSSSD with 16 vertical strips in the front side and 16 horizontal strips in the back side having a $500\,\mu$m thickness. The last stage is made of four CsI(Tl) crystals with a 6 cm thickness for the full stopping of energetic charged light particles [8].

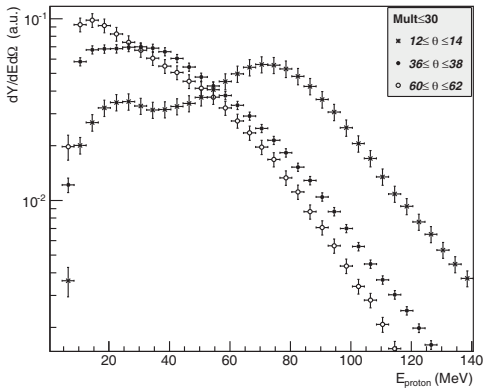

Fig. 2. – Protons energy spectra for different angular ranges and for less violent collisions for $Mult_{tot} \leq 30$ [9].

Central collision events, are selected by using the total charged-particle multiplicity ($Mult_{tot}$), that is the sum of the number of charged particles detected in LASSA plus the number of charged particles detected in the Miniball/Miniwall. Most of the following analysis deals with proton-proton correlations. By studying proton energy spectra, it is seen that for $Mult_{tot} < 30$ (quasi-peripheral events) the spectra show a strong contribution of a fast component at forward laboratory angles between 12° and 14° fig. 2; in fact a broad bump is clearly observed, ranging roughly between 60 and 90 MeV, and peaked to a value of about 70 MeV, corresponding to a value of proton velocity nearly 14% larger than the beam one. They are interpreted as protons emitted by the fast moving source of the quasi-projectile superimposed with a fast pre-equilibrium component. Both the value of the peak and the broadness of the distribution are strong indications of sizeable effects in the spectra coming from quasi-projectile emission of a kinematical convolution of the Fermi motion with the beam velocity. At backward angles, between 40° and 60°, fig. 3, the spectra are enriched by a lower-energy proton component, indicating slow-moving sources created in the overlapping region of the collision pattern and having a velocity intermediate between the projectile and the target.

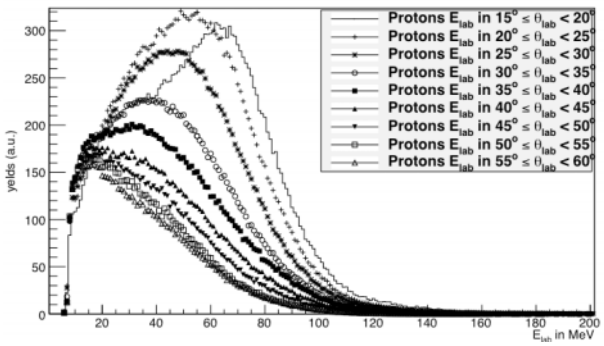

Fig. 3. – Protons energy spectra for different angular regions in lab frame for all $Mult_{tot}$.

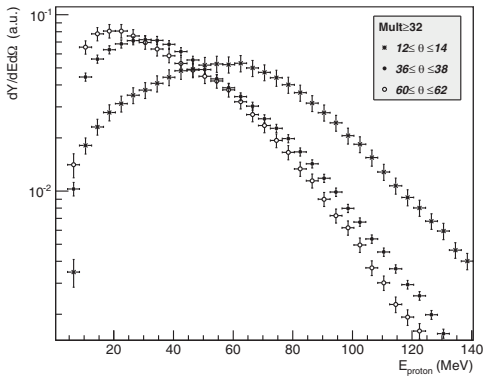

Fig. 4. – Violent collisions proton energy spectra for different angular regions $Mult_{tot} \geq 32$ [9].

The presence of the fast component is strongly reduced by selecting the most violent collisions when analysing spectra with high values of the particle multiplicity, *i.e.*, $Mult_{tot} > 32$, fig. 4.

However, in our analysis we have chosen the less restrictive condition of $Mult_{tot} > 25$ in order to take into account for a compromise between centrality and collected statistic fig. 5. We can see, by inspecting fig. 5, that the fast quasi-projectile component is strongly suppressed. The spectra of fig. 5 (in particular at backward angles) are interpreted as due to the presence of two possible emitting sources: a fast one due to the pre-equilibrium emission, and a second one, slow, due to the contribution of the, late, stages of the reaction (evaporations, secondary decay, etc.).

Having these selections in mind, in the following of the paper the proton-proton correlation function of the studied reaction will be discussed in some details.

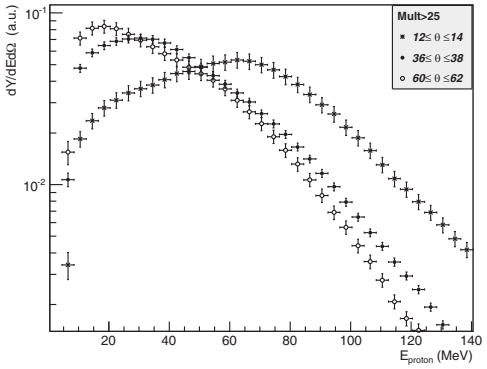

Fig. 5. – Energy spectra at three selected angular regions for $Mult_{tot} \geq 25$ (see text for explanations) [9].

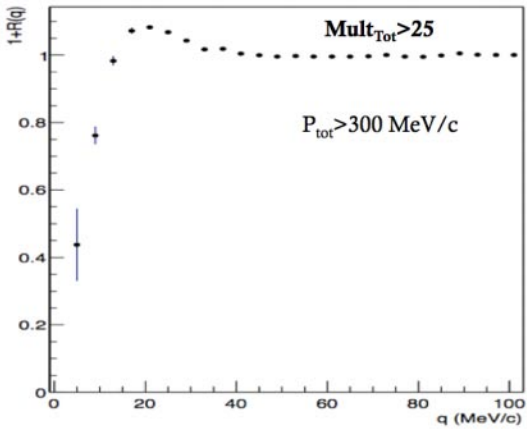

Fig. 6. – Proton-proton correlation function in Xe + Au 50 MeV/nucleon [9].

3. – Proton-proton correlation function method

In fig. 6 the proton-proton correlation function (see below for the description) is shown. As already suggested in the previous chapter, the correlation function shown on fig. 6 includes contributions of protons emitted by different emitting sources: a fast(pre-equilibrium) source and a slow evaporating and secondary decay source.

The experimental correlation function, $1 + R(\mathbf{q})$, is defined by the following equation:

$$Y_{12}(\mathbf{p}_1, \mathbf{p}_2) = C_{12} \cdot [1 + R(\mathbf{q})] \cdot Y_1(\mathbf{p}_1) \cdot Y_2(\mathbf{p}_2), \tag{1}$$

where $Y_{12}(\mathbf{p}_1, \mathbf{p}_2)$ is the coincident yield of the two particles detected in the same event, and C_{12} is a normalization constant obtained by imposing that $R(\mathbf{q}) \approx 0$ for very large values of relative momentum, $\mathbf{q}$, of the two particles; and the quantities $Y_1(\mathbf{p}_1)$ and $Y_2(\mathbf{p}_2)$ are the single-particle yields of the two particles. Theoretically the proton-proton correlation function is calculated by the koonin-Pratt integral equation:

$$1 + R(\mathbf{q}) = 1 + \int \mathrm{d}\mathbf{r} S(\mathbf{q}) \cdot K(\mathbf{r}, \mathbf{q}). \tag{2}$$

$S(\mathbf{q})$ is the source function and it is defined as the probability to emit two protons at the relative particle-particle distance r, calculated at the time when the second proton is emitted; the function $K(\mathbf{r}, \mathbf{q})$ is the kernel of the integral equation and it contains the ingredients of the final state interactions (FSI, Coulomb + Nuclear) and quantum statistics effects (dealing with two identical fermions). In order to characterize the emitting source we first used a Gaussian approach, by assuming a Gaussian size shaped source function, as follows:

$$S(\mathbf{q}) \propto e^{-\frac{r^2}{2r_0^2}}. \tag{3}$$

To take in to account and to illustrate the contribution of the different emitting time-scales, the source function is split in two contributions fast and slow, and the corresponding correlation functions are shown on fig. 7.

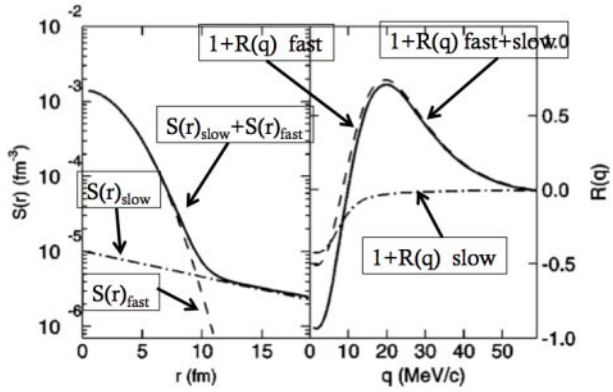

Fig. 7. – Comparison between a fast-emitting source function and a slow-emitting source function with their sum (left side), and their corresponding correlation functions [10] (right side).

The main contributions of the slow emitting source is found at low values of the relative momentum ($q < 20\,\mathrm{MeV}/c$) where, from an experimental point of view, it is necessary to have very good resolution (essentially angular resolution) to constrain the theoretical predictions. In the experiment described in this paper, the resolution was not enough to efficiently detect (see fig. 11) pairs of protons with such a low values of the relative momentum. In order to describe the relative importance of the fast and slow components and to take into account the difficulty in detecting pairs of protons at low values of relative momentum, a modified Gaussian source function has been used:

$$S(\mathbf{q}) = \frac{\lambda}{(2\pi)^{\frac{3}{2}} r_0^3} e^{-\frac{r^2}{2r_0^2}}. \tag{4}$$

In eq. (4), r_0 is the size parameter (as in eq. (3)) and λ is the fraction of proton-proton pairs emitted only by the fast emitting source. In the literature the height of the correlation peak has been commonly linked to the size of the emitting source. As a matter of fact, calculations on fig. 8 show that such link is possible if one assumes that $\lambda = 1$, *i.e.*, if all proton-proton pairs were emitted by the fast emitting source.

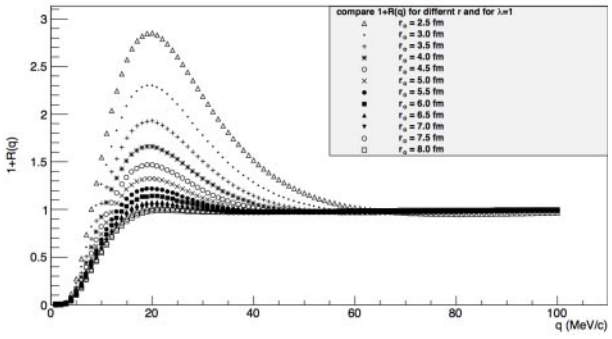

Fig. 8. – Comparison among correlation functions for different size of the emitting source [9].

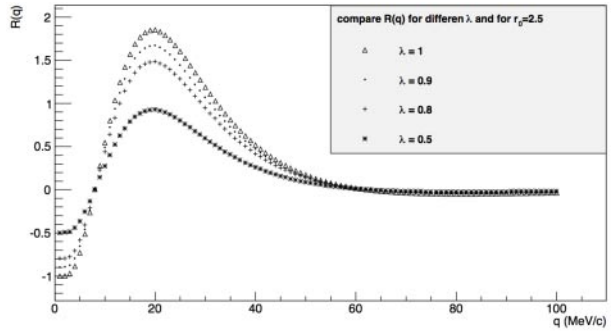

Fig. 9. – Comparison among correlation functions having the same size but different lambda parameter [9].

Clearly, for $\lambda = 1$, the larger is the height of the resonant peak, the smaller is the size of the emitting source. Unfortunately, if the lambda parameter is progressively reduced and the size is fixed ($r_0 = 2.5\,\mathrm{fm}$ in the case of fig. 9) the calculated correlation functions show the same trend of fig. 9.

This very simple model shows that different pairs of values for λ and r_0 predict practically identical heights of the resonant peak (see fig. 10). However, significant different values of the width correlation functions are observed. For this reason, in order to extract a realistic value of the size, it is important to measure with high accuracy the overall shape of the correlation function.

To further illustrate this delicate aspect of the analysis, the experimental correlation function (eq. (1)) was fitted using the formalism of the eq. (2), using the two parameter Gaussian described by eq. (4).

On fig. 11 the parameter λ was fixed to the value of 1 and the best fit produced a value of $r_0 = 6.3\,\mathrm{fm}$. Unfortunately the quality of the fit prediction is very poor, with a low test-value of the chi-square, $\chi^2 = 7.45$. In contrast, on fig. 12 a new best-fit of the data is shown, where both free parameters λ and r_0 are used.

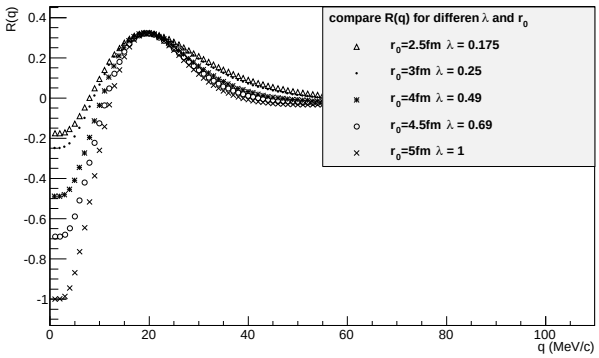

Fig. 10. – Comparison among $R(q)$ having different size and lambda, but with the same peak height [9].

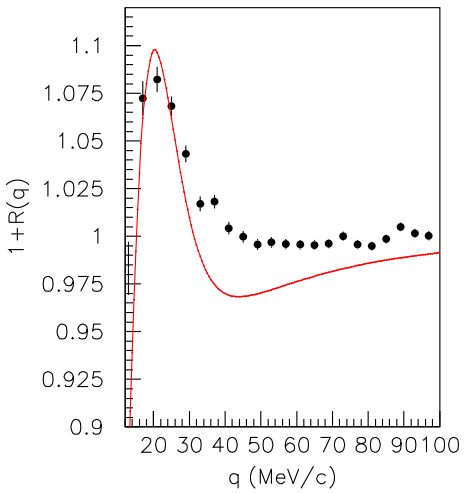

Fig. 11. – Gaussian fits of the experimentally correlation function $\lambda = 1$ [9].

In this case a better agreement between the fit and the experimental data is achieved, confirmed by a larger test-value of the chi-square, $\chi^2 = 0.96$. The values of the size and of the parameter λ are, respectively, $r_0 = 5.6\,\mathrm{fm}$ and $\lambda = 0.48$. This latter best-fit predicts a slight smaller size of the source and a strong reduction (about 50%) of the intensity of the fast component of proton-proton pairs. In order to extract physics information in a less model-dependent fashion the analysis is continued by applying Imaging techniques [10]. The Imaging technique consists in a numerical inversion of the Koonin-Pratt equation, eq. (2). The numerical inversion allows to extract the source function without any assumptions on its functional profile. The inversion method allows to extract the corresponding profile of the source (see right side of fig. 13). The size of the emitting source (evaluated as the value of FWHM on fig. 13 and fig. 14) takes the value of size $r_{\frac{1}{2}} = 4.4(\pm 0.3)\,\mathrm{fm}$ and it is smaller than the one extracted by means of the

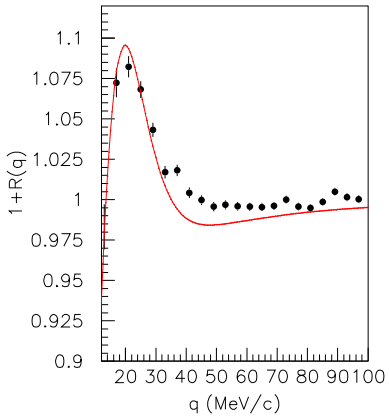

Fig. 12. – Gaussian fit of the experimentally correlation function, with λ parameter free [9].

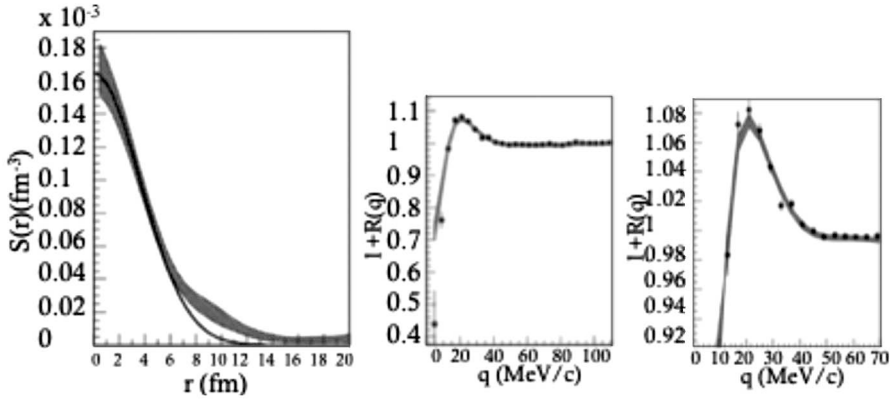

Fig. 13. – Left panel: $S(r)$ extracting by imaging. Right panel: the corresponding correlation function tescribing the experimental correlation function (full dots) [9].

Gaussian assumption. The value of the λ parameter is smaller too, with a value of and $\lambda = 0.18$. This value was consistently estimated by using the following relation:

$$\lambda_{fast} = 4\pi \int_0^{2.5r_{\frac{1}{2}}} S(\mathbf{q}) r^2 \mathrm{d}r. \tag{5}$$

So, the model-independent inversion technique produces slight smaller size of the source than expected by the Gaussian fit assumption and, more important, it shows a fast component of about 20% of the total intensity of the proton-proton pairs emitted by the system. This fractions indicates that about 45% of protons originate from fast-emitting source in the dynamic evolution of the source. On fig. 14 a comparison between the Gaussian fit evaluation and the imaging source technique result is shown.

By inspecting fig. 14, one observes that for values of the radius r of the source profile smaller than about 6 fm, the Gaussian fit method is in agreement with the Imaging Technique evaluation. However significant deviations are seen for larger value of the radius r. A consistent interpretation with the source profile concept suggests these large values of the radius of the source profile of the imaging technique as due to the presence

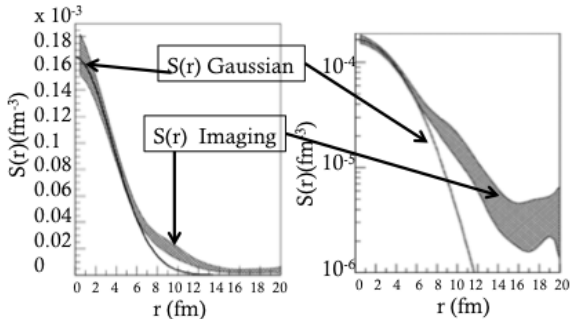

Fig. 14. – Comparison between Gaussian (solid line) and imaging source functions [9].

of longer emission time-scale overlapped on fast dynamical contributions. The analysis reveals strong evidence for sizeable intensity for a secondary long-lived decay, associated with a slow process linked with a de-excitation to the ground state of excited nuclei produced in the final state, as is confirmed by the shape of the energy spectra on fig. 2 and fig. 3 clearly revealing the presence of multiple emission mechanism.

4. – Conclusions

In this article a particle-particle correlation analysis and its use to understand some of the properties of proton emission mechanisms are reported. It is shown that powerful methods to analyse the detailed line-shape of two-proton correlation functions are an important condition to disentangle between pre-equilibrium emission and slow decay processes in the reaction mechanism. Furthermore, these techniques allow extracting the profile of the emitting sources, which is an important quantity to test transport models of heavy-ion collisions, as well as their space-time extent [11, 12]. A complete investigation of the emitting sources will require the extension of correlation and imaging techniques to other particle pairs, trying to keep under control the presence of collective motion that may significantly affect the apparent space-time properties of the source. Our study clearly stresses the necessity to improve the performance of the existing particle-particle arrays. In this perspective, the construction of a new array, FARCOS (Femtoscope Array for Correlations and Spectroscopy) [9] is presently in progress at the INFN, Sezione di Catania and Laboratori Nazionali del Sud.

REFERENCES

[1] Li Bao-An *et al.*, *Phys. Rev. C*, **71** (2005) 044604.
[2] Baran V. *et al.*, *Nucl. Phys. A*, **730** (2004) 329.
[3] Hudan S. *et al.*, *Phys. Rev. C*, **67** (2003) 064613.
[4] Liu T. X. *et al.*, *Phys. Rev. C*, **69** (2004) 014603.
[5] Tan W. P. *et al.*, *Phys. Rev. C*, **64** (2001) 051901.
[6] Verde G. *et al.*, *Eur. Phys. J. A*, **30** (2006) 81.
[7] Satcheler G. R., *Introduction to Nuclear Reactions* (The Macmillan Press Ltd) 1980, pp. 15, 71 (ISBN 0-333-25907-6).
[8] Davin B. *et al.*, *Nucl. Instrum. Methods A*, **473** (2001) 302.
[9] Pagano E. V., *Tesi di Laurea Magistrale in Fisica Nucleare*, A.A. 2011-2012.
[10] Verde G. *et al.*, *Phys. Rev. C*, **65** (2002) 054609.
[11] Verde G. *et al.*, *Phys. Rev. C*, **67** (2003) 034606.
[12] Kunde G. J. *et al.*, *Phys. Rev. Lett.*, **70** (1993) 2545.